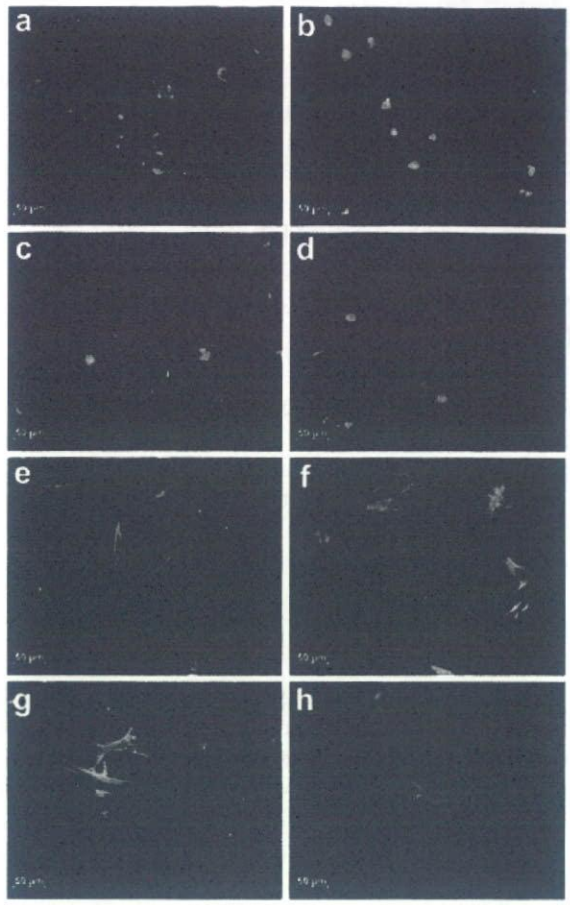

Fig. 3. Adhesion of hBMSC, 30 min, 1, 4, and 24 h after seeding. **a**, **c**, **e**, **g** (*left row*) mineralised collagen membrane, **b**, **d**, **f**, **h** (*right row*) demineralised collagen membrane. **a**, **b** 30 min, **c**, **d**: 1 h, **e**, **f**: 4 h, **g**, **h**: 24 h after seeding. Fluorescence micrographs; samples were fixed and stained with Alexa Fluor488 phalloidin for cytoskeleton and DAPI for nuclei; *scale bars* = 50 µm

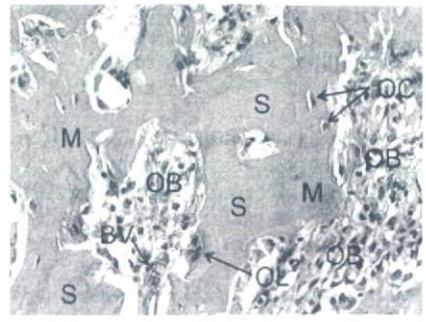

Fig. 4. Histological image of a porous 3D scaffold made of mineralised collagen, 2 weeks after implantation in a bone cavity of rat femur. HE stain, ×100. *S* scaffold, *M* newly deposited bone matrix, *OB* osteoblasts, *OC* osteocytes, *OL* osteoclast, *BV* blood vessel

surface of the scaffold. In the newly deposited matrix some osteocytes are embedded. Remaining scaffold material is resorbed by osteoclasts (proven by TRAP staining; images not shown). In the pores already blood capillaries can be found—showing that the interconnecting pore system is suitable for fast vascularisation.

Combining the mineralised collagen in the liquid (suspended) state with a (non-mineralised) collagen hyaluronic acid composite, followed by joint freeze–drying and chemical crosslinking, biphasic, but monolithic scaffolds for the therapy of osteochondral defects could be achieved [7].

Calcium phosphate bone cements, functionalised with mineralised collagen

Addition of mineralised collagen fibrils to the solid precursor phase of a hydraulic calcium phosphate bone cement leads to a cement paste with better cohesion and an improved performance in vitro [8, 9] and in vivo [11]. Collagen acts as a fibre reinforcement of the brittle cement phase and improves the fracture toughness after hardening of the material. Presently, the cement is tested in a critical size defect model in the lower jaw bone of mini pig.

4 Discussion

Applying different methods for scaffold fabrication, we were able to develop several biomaterials out of mineralised collagen fibrils—a material which mimics ECM of healthy bone tissue. A review on other materials based on collagen HAP composites was recently given by Wahl et al. [12]. The scaffolds were proven to be biocompatible and showed good results in cell culture as well as in animal experiments. By co-culturing osteoblasts and osteoclasts on artificial ECM of bone in vitro models for bone remodelling can be established [10].

References

1. Rho JY, Kuhn-Spearing L, Zioupos P (1998) Med Eng Phys 20:92–102
2. Bradt JH, Mertig M, Teresiak A, et al (1999) Chem Mater 11:2694–2701
3. Burth R, Gelinsky M, Pompe W (1999) Tech Text 8:20–21
4. Bernhardt A, Lode A, Boxberger S, et al (2007) J Mater Sci Mater Med (in press). doi:10.1007/s10856-006-0059-0
5. Gelinsky M, König U, Sewing A, et al (2004) (in German). Materialwiss Werkstofftech 35:229–233
6. Yokoyama A, Gelinsky M, Kawasaki T, et al (2005) J Biomed Mater Res B Appl Biomater 75B:464–472
7. Gelinsky M, Eckert M, Despang F (2007) Int J Mater Res 98:749–755
8. Knepper-Nicolai B, Reinstorf A, Hofinger I, et al (2002) Biomol Eng 19:227–231
9. Hempel U, Poppe M, Reinstorf A, et al (2004) J Biomed Mater Res B Appl Biomater 71B:130–143
10. Domaschke H, Gelinsky M, Burmeister B, et al (2006) Tissue Eng 12:949–958
11. Schneiders W, Reinstorf A, Pompe W, et al (2007) Bone 40:1048–1059
12. Wahl D, Czernuszka JT (2006) Eur Cell Mater 11:43–56

9
Biochemical and Pathological Responses of Cells and Tissue to Micro- and Nanoparticles from Titanium and other Materials

Fumio Watari, Kazuchika Tamura, Atsuro Yokoyama, Kenichiro Shibata, Tsukasa Akasaka, Bunshi Fugetsu, Kiyotaka Asakura, Motohiro Uo, Yasunori Totsuka, Yoshinori Sato, and Kazuyuki Tohji

Abstract

Biocompatible titanium (Ti) causes inflammation when in the form of abraded fine particles, whereas asbestos, which is a type of clay mineral, induces mesothelioma after long-term, high-level exposure. In addition to these materials' properties, such as toxicity or biocompatibility, these phenomena may be seen to occur as a result of the "particle effect". The cytotoxicity of fine particles of Ti, Fe, Ni and TiO_2 was investigated *in vitro* using human neutrophils as probe cells, and also with the tissue reaction *in-vivo* implantation test. Biochemical functional analyses of cell survival rate, lactate dehydrogenase (LDH) activities, superoxide anion, cytokines and the microscopic observation of cellular morphology showed that the stimulatory effects on neutrophils and inflammation in soft tissue became more prominent as the particle size became smaller (<100 μm). Moreover, such effects were especially pronounced for particles <10 μm (about cell size), when phagocytosis was induced. Inductively coupled plasma elemental analysis showed dissolution from Ti particles to be negligible. Results with Fe were quantitatively similar to those with Ti, despite Fe being soluble. Taken together, these results indicated that the stimulus produced is based, non-specifically, on the physical size and shape effect of particles, and is more pronounced on the micro/nano scale. This is different from the material-dependent, chemical toxicity effects that are caused by ionic dissolution and normally dominant in bulk materials.

Key words: nanotoxicology, biocompatibility, titanium, superoxide, cytokine, neutrophil, macrophage, phagocytosis.

Handbook of Biomineralization. Edited by M. Epple and E. Bäuerlein
Copyright © 2007 WILEY-VCH Verlag GmbH & Co. KGaA, Weinheim
ISBN: 978-3-527-31806-3

9.1 Introduction

Metallic titanium (Ti) is highly corrosion-resistant due to the presence of a thin and stable protective oxide layer which forms on its surface. Moreover, it is one of the most biocompatible metals known to mankind [1, 2], and hence is regarded as the near-ideal material for implantation, being used widely in orthopedics and dentistry. Unfortunately, Ti has a weak point in that it has a low abrasion resistance [3, 4], whereby abraded fine particles produced from the sliding parts of artificial joints often cause inflammation in the surrounding tissues.

The reason why this material behaves in different ways depending on its particle size is unclear. By comparison, asbestos – a silicaceous clay-type mineral – induces mesothelioma after long-term, high-level exposure. These phenomena may originate not only from the material's biological properties, such as toxicity or biocompatibility, but also from particulate effects, including physical size and morphology.

Recently, significant advances have been made in the development of a drug delivery system (DDS) to administer anticancer agents and to conduct gene transfections. In this regard, it is essential to establish an understanding of the principles involved, and of the biological reactivity of micro/nanoparticles when developing these biomedical applications.

In this chapter we present details of studies aimed at determining the effects of fine particles, in terms of their size, on cytotoxicity *in vitro* and biocompatibility *in vivo*. These investigations included biochemical functional analyses with human neutrophils as probe cells, as well as histological observations in animal implantation tests [5–7]. In this way, the effects of Ti, Fe, Ni and TiO_2 particles could be compared directly.

Human neutrophils, which play a central, non-specific role in the initial stages of inflammation resulting from contact with a foreign body(ies), were used as probes. Particles that were either smaller (0.5 to 3 μm) or larger (10, 50, and 150 μm) than neutrophils were used to determine the relationship between cell or particle size and cytotoxicity.

9.2 Materials and Methods

9.2.1 Specimens

Ti, Fe, Ni and TiO_2 particles of 99.9% purity and of various sizes (from 300 nm to 150 μm) were used in these experiments. In order to equate experimental conditions between materials of the particle group, particles of 0.5, 3 and 10 μm were extracted by sedimentation, while those <300 nm in size were extracted by ultra-

filtration. Fullerene (C_{60}), multiwalled carbon nanotubes (CNT) and hat-stacked carbon nanofibers (CNF) – a derivative of CNTs – were used for some additional experiments.

9.2.2
Dissolution Testing of Ti Particles

After immersion of Ti particles in Hank's balanced salt solution (HBSS) at 37 °C for one month, the suspension was filtered through a 0.45-μm pore membrane to remove Ti particles. The supernatant was then analyzed using inductively coupled plasma-atomic emission spectrometry (ICP-AES) elemental analysis (ICPS-8100; Shimazu, Tokyo, Japan).

9.2.3
Probe Cells

Neutrophils were separated from human peripheral blood obtained from healthy volunteers, using 6% isotonic sodium chloride containing hydroxyethyl starch and lymphocyte isolation solution (Ficoll-Hypaque™; Amersham Pharmacia Biotech AB, Sweden). After mixing with HBSS, the particles were maintained at 37 °C, the neutrophils added, and the whole mixture was used for a variety of cell toxicity tests. A human acute monocytic leukemia cell line (THP-1) was also used for additional experiments.

9.2.4
Biochemical Analyses of Cellular Reactions to Materials

Cell survival rates, LDH activities and superoxide anion (O^{2-}) production per 10^6 neutrophils were measured. Cytokines of tumor necrosis factor alpha (TNF-α) and interleukin 1β (IL-1β) were measured using ELISA kits (Endogen, Inc., USA). Morphological changes of neutrophils mixed with HBSS and containing various particles were observed using optical microscopy (OM) (Zeiss Axioskop; Germany) and scanning electron microscopy (SEM) (Hitachi S-4300; Tokyo, Japan).

9.2.5
Animal Experiments

Particles were inserted into the subcutaneous connective tissue of the abdominal region of Wistar rats (aged 11–12 weeks; body weight 350–380 g). Specimens were prepared through the usual process of fixation, embedding, sectioning, and staining with hematoxylin and eosin, and then observed histopathologically. A compulsory exposure test was also performed using 30-nm TiO_2 particles. The observation of internal diffusion of nanoparticles was conducted by elemental mapping in air using X-ray scanning analytical microscopy (XSAM) (Horiba

XGT-2000V; Tokyo, Japan) without the pretreatments of fixation, dehydration and staining after sectioning.

9.3 Results

9.3.1 Dependence of Tissue Reaction *In Vivo* on Material Macroscopic Size

A comparison of tissue reaction with macroscopic size (1 mm × 10 mm) of Ni, Ti, Fe and Ag after one week of implantation in the dorsal thoracic region of rats is shown in Figure 9.1. In each case, the implant was originally situated in the upper space. With Ni, there was an expansion of capillary vessels, and the tissues in the distant regions became necrotic and degenerated. Fibrous connective tissue surrounding the implant was already formed for Ti and Fe from the earlier stage, and was still in the course of formation for Ag at this stage. Such a comparison highlights the different sensitivities of biocompatibility of these metals [5].

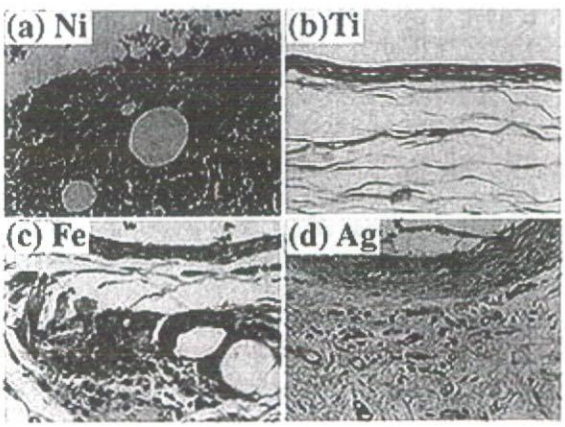

Fig. 9.1 Histological image of rat soft tissue after one-week implantation with (a) Ni, (b) Ti, (c) Fe and (d) Ag particles of macroscopic size (1 mm × 10 mm).

9.3.2 Effect of Particle Size on Biocompatibility

9.3.2.1 Size Distribution of the Abraded Particles

A typical example of size distribution of abraded particles from Ti, produced by grinding with a dental air turbine, is shown in Figure 9.2. The largest proportion of particles were approximately 5 μm in size, followed by 0.8 μm, 0.2 μm, and

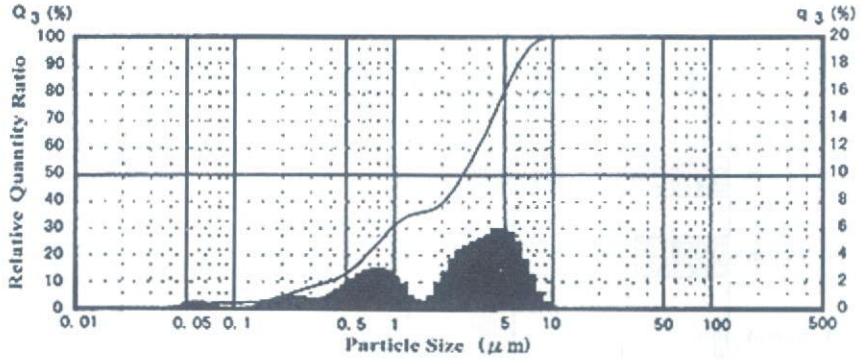

Fig. 9.2 Typical size distribution of abraded particles of Ti produced by grinding with a dental air turbine.

0.07 μm. These more sensitive particle sizes, based on biological reaction, were further investigated in the following sections.

9.3.2.2 Particle Size Dependence *In Vitro*

The survival rate of human neutrophils in HBSS containing Ti particles is shown graphically in Figure 9.3, with HBSS solution used as the control. The average

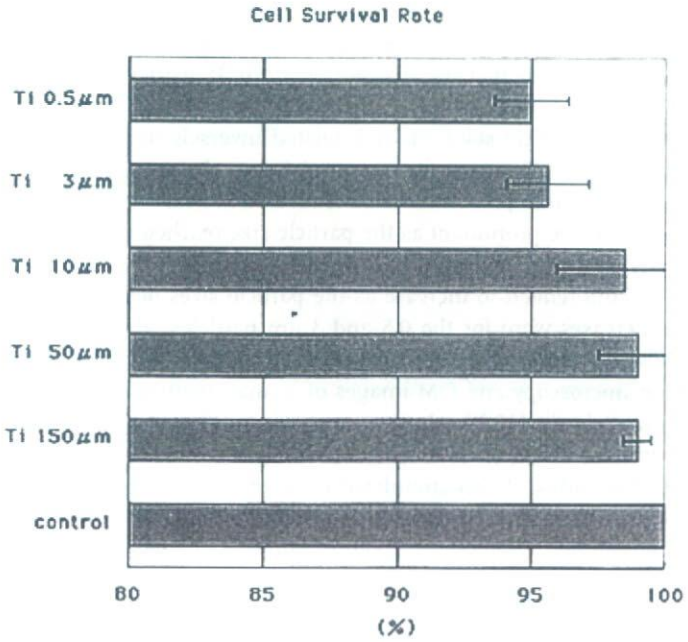

Fig. 9.3 Dependence of cell survival rate on Ti particle size [6].

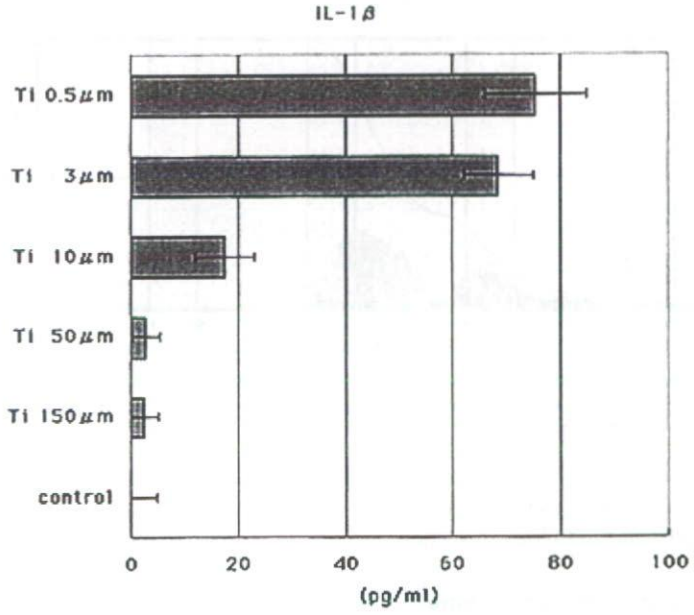

Fig. 9.4 Dependence of interleukin (IL)-1β release from neutrophils on Ti particle size [6].

survival rate was seen to decrease in line with decreases in particle size, with significant differences from control being observed for the 0.5 and 3 μm particles. ICP elemental analysis showed that the dissolution from Ti particles was negligible (i.e., below detection limits) [6].

LDH activities in each particle solution were related inversely to the cell survival rate, with significant differences from control being observed for the 0.5 and 3 μm particles. Superoxide production also tended to increase with decreasing particle size, and became prominent as the particle size reached <10 μm.

Interleukin-1β release from neutrophils in HBSS containing Ti particles is shown in Figure 9.4, and tended to increase as the particle sizes decreased. The most pronounced increases were for the 0.5 and 3 μm particles. The release of cytokine TNF-α showed a similar behavior to that for IL-1β.

Scanning electron microscopy and OM images of human neutrophils exposed to Ti, TiO_2 and Ni particles in HBSS solution are shown in Figure 9.5. The morphology of the neutrophil in HBSS as a control (see Fig. 9.5a) changes, depending on the degree of stimulus. When stimulated by 0.5 or 3 μm Ti particles, the neutrophil surface was changed to become either knobbly or smooth, by transformation of the cell membrane. In addition, a neutrophil may extend its pseudopodia in order to phagocytose a TiO_2 or Ti particle (Fig. 9.5c,d); the particles already phagocytosed can be observed inside the cell (Fig. 9.5d). The morphology of neutrophils exposed to Ni particles was generally either transformed or destroyed (Fig. 9.5b). In the case of Ti particles larger than 10 μm, phagocytosis was not

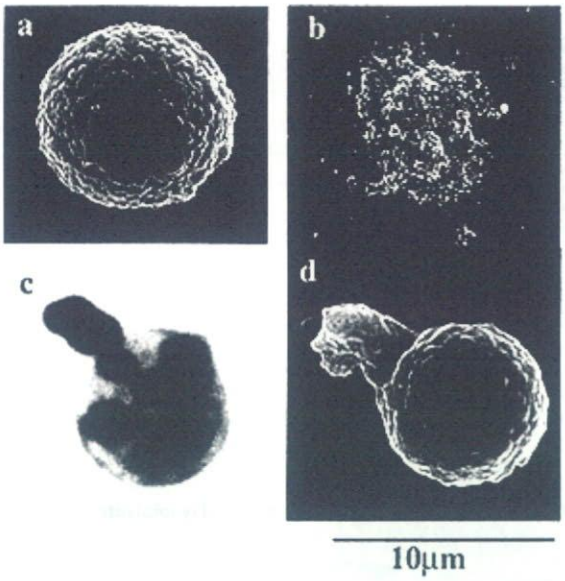

Fig. 9.5 (a,b,d) Scanning electron microscopy and (c) optical microscopy images of human neutrophils. (a) Control neutrophil in HBSS; (b) after exposure to particles of Ni (500 nm); (c) after exposure to TiO_2 particles (300 nm); (d) after exposure to Ti particles (500 nm) [6].

observed and the form of the neutrophils was changed only minimally. The pronounced phenomena of biochemical cell reactions observed for particle sizes below 10 µm (see Figs. 9.3 and 9.4) were closely related to the phagocytosis (Fig. 9.5).

9.3.2.3 Particle Size Dependence *In Vivo*

A series of *in-vivo* tests showed that Ti particles larger than 100 µm were surrounded by a fibrous connective tissue layer, which is the usual reaction for biocompatible materials such as the bulk size of a Ti implant. As the particle sizes became smaller, inflammation was seen to occur; however, the presence of particles < 10 µm (about cell size) caused phagocytosis by macrophages to be induced. Numerous inflammatory cells were observed in the surroundings of the Ti particles, and both macrophages and neutrophils showed degenerative changes in their morphology [7].

The histological images of rat soft tissues into which 3 µm and 10 µm Ti particles had been inserted for 5 days are shown in Figure 9.6. In the case of the 3 µm particles, macrophage-based phagocytosis had occurred and the Ti particles were observed inside the cells, such that the cytoplasm of an inflammatory cell contained numerous small black particles. In contrast, the 10 µm Ti particles were seen to locate outside the cells, with phagocytosis rarely being observed and the tissue showing a much lesser degree of inflammation.

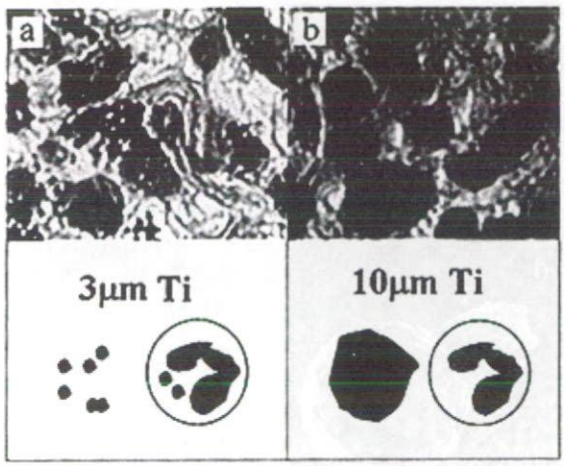

Fig. 9.6 Tissue reaction to (a) 3 μm and (b) 0.5 μm Ti particles after 5-day implantation.

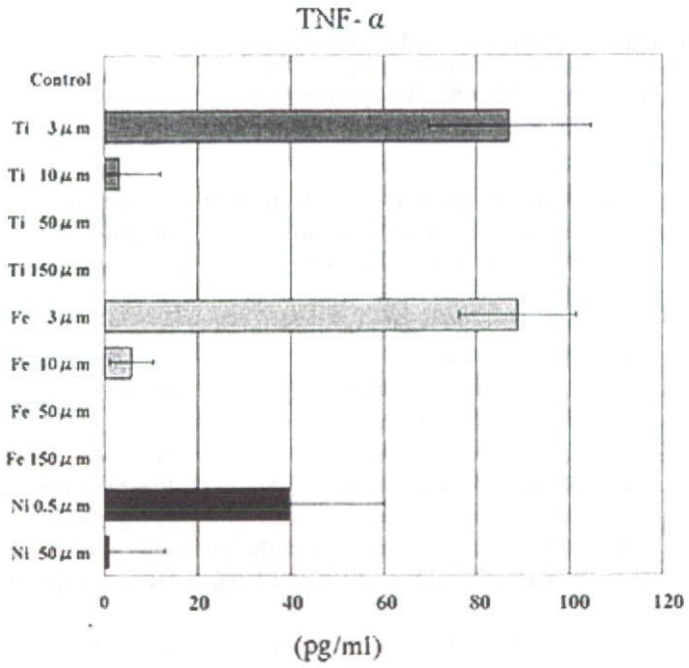

Fig. 9.7 Dependence of TNF-α release from neutrophils on particle size for Ti, Fe, and Ni.

9.3.2.4 Material Dependence of the Particle Size Effect *In Vitro*

The comparative release of TNF-α by Ti, Fe and Ni particles is illustrated graphically in Figure 9.7. Both, Ti and Fe particles, showed a tendency towards increased TNF-α release as the particle size decreased (and to similar degrees), whereas Ni demonstrated a particle size-dependent release, with relatively lower values. Of note, the behavior of Fe was almost equal to that of Ti in a quantitative sense, despite clear differences in the chemical properties of these two materials. Interleukin-1β, superoxide anion and LDH production showed, likewise, a similar tendency to increase compared to a decrease in particle size for both Ti and Fe.

Ni also demonstrated a particle size-dependency in the cell functional tests, although the quantitative values obtained differed from those obtained with Ti and Fe. Typically, the cell survival rate was significantly lower than in controls, but LDH activity was higher. However, the degree of superoxide anion and IL-1β production was less with Ni than with Ti and Fe.

9.3.2.5 Material Dependency of Tissue Reaction to Particles *In Vivo*

Comparative histopathological observations of the soft tissues of rats into which 3 µm particles of Ti, Fe and Ni were inserted for 5 days are shown in Figure 9.8.

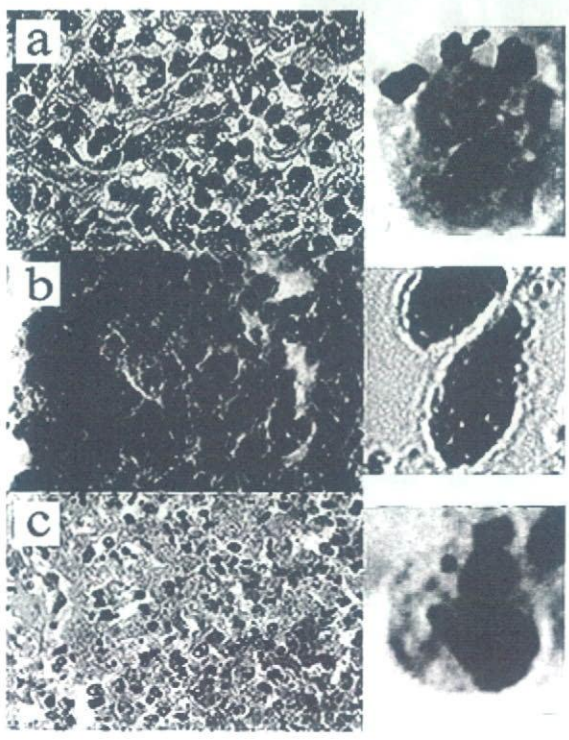

Fig. 9.8 Histopathological observation of *in-vivo* reaction to 3 µm particles. (a) Ti; (b) Fe; (c) Ni.

Macrophage-based phagocytosis was effected for both Ti and Fe particles, while necrosis occurred in the case of Ni particles.

9.3.3
Shape Effect

Scanning electron microscopy images of a set of massive and acicular TiO_2 particles, of equivalent diametric size and longitudinal length (ca. 10 μm), are shown in Figure 9.9. The subsequent particle size-dependence of IL-1β release from neutrophils for these TiO_2 particles is illustrated graphically in Figure 9.10. TNF-α

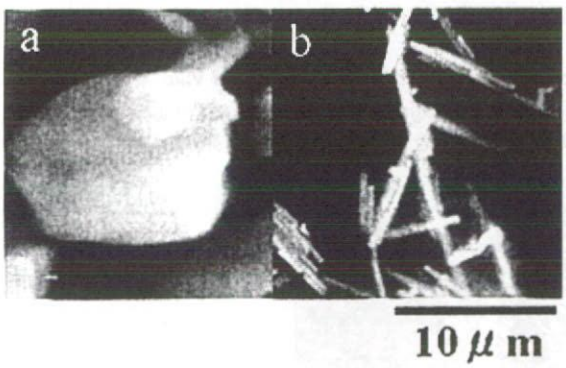

Fig. 9.9 Scanning electron microscopy images of massive and acicular TiO_2 particles with equivalent diametric size and longitudinal length, respectively.

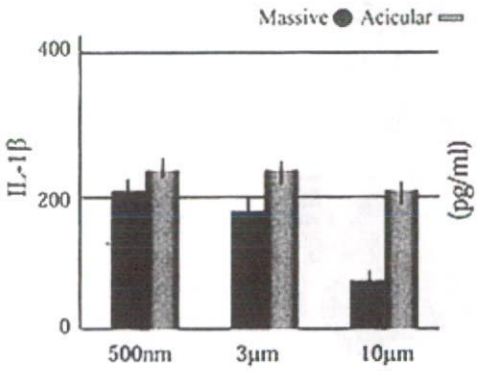

Fig. 9.10 Particle size dependence of IL-1β release from neutrophils for massive and acicular TiO_2 particles.

release, which is related to phagocytosis, showed very similar size-dependencies for both massive and acicular particles, but for IL-1β the massive particle shape showed a dependency similar to that for TNF-α, where cytokine production was enhanced below a particle size of 10 μm, but reduced for particles > 10 μm (Fig. 9.10). In contrast, production levels of IL-1β remained high for 10 μm acicular particles, indicating that this type of particle has a more stimulatory role than do massive particles. Of note, IL-1β represents a different type of stimulus and inflammation compared to TNF-α, despite both cytokines being indicators of inflammation.

9.3.4
The Origin of the Particle Size Effect

For the same material, it is clear that cell and tissue reactions differ between the bulk state and fine particles. The results of both *in-vitro* biochemical cell functional tests and *in-vivo* animal tests were in accordance with the finding that, when in bulk, even biocompatible materials such as Ti and TiO_2 become stimulatory as their particle size is decreased, and that this is especially pronounced below a size of 10 μm, when phagocytosis is induced. The relationship between cell/tissue and particle size is shown schematically in Figure 9.11. The cell-stimulatory and tissue-inflammatory natures of particles, as described above, originate from the relative size relationship between the particle and the cell/tissue. Previously, these phenomena were characterized as non-specific cytotoxicity aris-

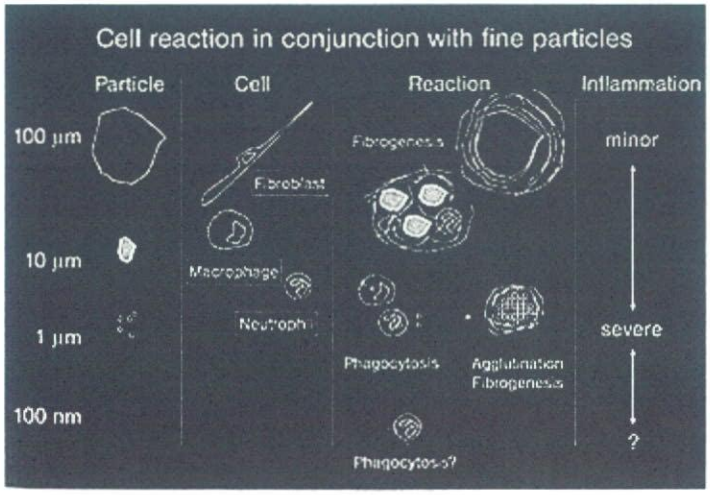

Fig. 9.11 The relationship between cell/tissue and particle size.

ing from physical size effects; these differ from chemical toxicity effects, which are based on ionic dissolution and usually are dominant in bulk materials.

9.3.5
Toxicity Level of Particle Size Effect for Bioactive and Bioinert Materials

The comparative production of TNF-α in THP-1 cells (a human acute monocytic leukemia cell line) following treatment with fullerene (C_{60}), carbon nanofibers (CNFs) and lipopeptide, is shown graphically in Figure 9.12. Clear differences were apparent in TNF-α production among CNFs, depending on the treatment conditions utilized (whether acid- or CHAPS-treated) [8]. CNFs, which are derivatives of CNTs, have a crystal structure in which a graphene sheet forms a circular cone, with several cones being stacked towards the needle-axis. C_{60}, CNFs and CNTs [9–17] are bioinert materials that show similar behavior to Ti or TiO_2 in terms of both cell functional tests and size-dependence, leading to inflammation in the tissues *in vivo* [18–22].

The diacylated lipopeptide FSL-1 was used as a positive control, as it is known to induce macrophages to produce TNF-α. The concentration of C_{60} and CNFs was 0.1 to 10 μg mL^{-1}, and that of the lipopeptide 10 ng mL^{-1}. Although the dose of lipopeptide was much lower, the level of activation of THP-1 cells was far beyond that of C_{60} and CNFs. This implied that the stimulatory level by bioactive and bioinert materials was far lower (perhaps 1/1000th to 1/10 000th) compared to the toxicity level of microbial lipopeptide, which is a type of bacterial endotoxin. It should be recognized, however, that micro/nanoparticles still induce phagocytosis and inflammation.

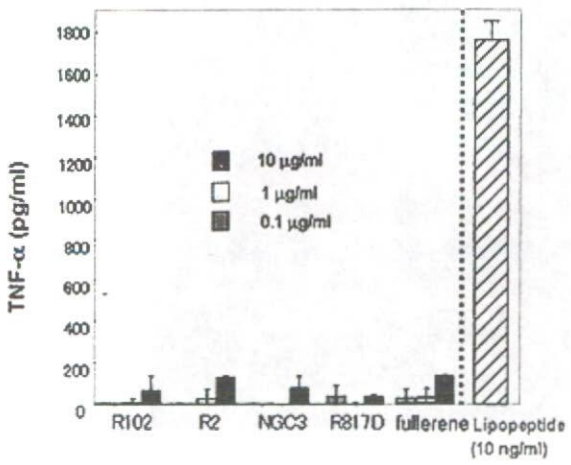

Fig. 9.12 Comparison of TNF-α release for carbon nanofibers and endotoxin (lipopeptide) [8].

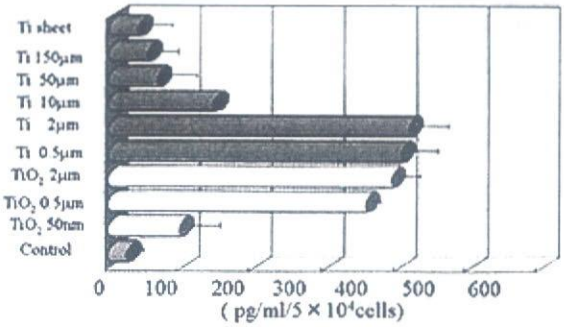

Fig. 9.13 Dependence of TNF-α release from neutrophils on particle size down to nanometer size.

9.3.6 Nanotoxicology

9.3.6.1 Size-Dependent Stimulus Down to Nanometer Size

The dependence on particle size (down to nanometer) of TNF-α release from neutrophils is shown graphically in Figure 9.13. Below a particle size of 0.5 μm, metallic Ti is difficult to treat as it is easily oxidized in air, and consequently TiO_2 was used to create a smaller particle size. Metallic Ti and TiO_2 showed similar dependencies, in both qualitative and quantitative manner, which reflected the non-specific properties of a stimulus induced by a particle size effect. The stimulus – in this case the amount of TNF-α released – was pronounced below a particle size of 10 μm, exhibited a maximum from a size of about 1 μm down to 0.5 μm, and decreased with sizes < 0.2 μm. Although the level of TNF-α release was low at the 50 nm particle size, this might be preferred for the biological use of nanoparticles, as the stimulus was decreased. In this situation, however, the biophylactic system would no longer function adequately to combat any invasion by nanoparticles.

9.3.6.2 Internal Diffusion of Nanoparticles

Nanoparticles (especially those <50 nm in size) may invade the internal body through either the respiratory or digestive systems. Figure 9.14 illustrates internal whole-body Ti mapping of rats, using X-ray analytical microscopy (XSAM), to show the distribution of 30-nm TiO_2 particles inside the body, following compulsory inhalational exposure. Condensation of the particles occurred from the respiratory system to the urinary bladder by diffusion in the whole body through the cardiovascular system, following direct uptake into blood vessels from the lungs.

It is likely that the existence of nanoparticles is not recognized by the body's defense system, and consequently an understanding of their behavior within the body is essential if they are to be used as effective drug delivery systems. Thus, it is important that the internal dynamics of particles be determined if nanoparticles are to be used in this way.

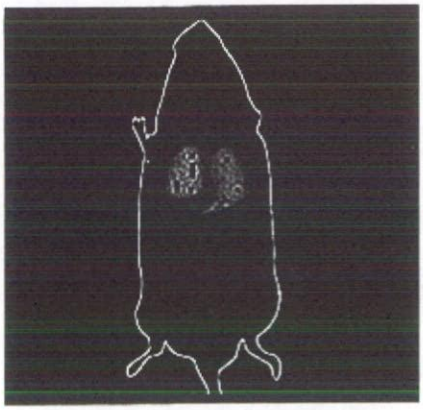

Fig. 9.14 X-ray scanning analytical microscopy Ti mapping of internal distribution of 30 nm TiO_2 particles after compulsory exposure test.

9.3.6.3 Toxicity-Enhancing Effects of Biostimulatory Materials by Nanosizing

Following a one-year implantation of 0.5 μm Ni particles, tumors were seen to occur in the subcutaneous tissues of rats (Fig. 9.15). Although Ni is known to be toxic when in macroscopic form (see Fig. 9.1), its toxicity is enhanced remarkably when in a fine-particle state. Such a specific surface effect increases reciprocally with particle size, and may lead to the enhancement of adverse chemical and toxic effects.

Fig. 9.15 Tumor induced after one-year implantation of 0.5 μm Ni particles.

9.4 Discussion

9.4.1 Particle Size-Dependence of Cytotoxicity

The results of these biochemical functional analyses and microscopic morphological observations showed cell survival to have decreased (see Fig. 9.3) and, corre-

spondingly, the activity of LDH (an indicator of cell disruption) to have been increased, as the Ti particle size was reduced from 150 μm to 0.5 μm. Both, superoxide anion and cytokine (IL-1β, TNF-α) production also tended to increase as particle sizes decreased, notably for those of 0.5 and 3 μm. Whilst superoxide anions are released from intracellular organs and cell membranes when stimulated, IL-1β is released when neutrophils are stimulated by foreign bodies, leading to the inflammation reaction cascade. TNF-α release is closely related to phagocytosis. Both, OM and SEM observations (see Fig. 9.2) indicated that only Ti particles of 0.5 and 3 μm were phagocytosed by neutrophils (which themselves were 5–10 μm in diameter), whereas phagocytosis proved to be difficult for the 10-, 50-, 150-μm Ti particles.

The results of cell survival (Fig. 9.3), LDH activity increase, superoxide production and release of IL-1β (Fig. 9.4) and TNF-α (Fig. 9.5) were shown to be particle size-dependent, with effects becoming more apparent as the particle size was reduced. This was especially pronounced when the size was less than that of the cell. ICP elemental analysis confirmed that dissolution from Ti particles was below the limits of detection, and effectively negligible; thus, the biofunctional changes demonstrated in the present studies were not caused by any chemical effects of the Ti ions but rather were due to physical size effects of the Ti particles.

9.4.2
Particle Size-Dependence in Soft Tissues

The *in-vivo* implantation of a variety of Ti particle sizes in the soft tissue of rats showed that particles > 100 μm were surrounded by a fibrous connective tissue layer, this being the normal reaction for biocompatible materials such as a Ti implant. Particles < 100 μm in size tended to cause inflammation, but this was even more pronounced for smaller particles. Particles of <10 μm – about cell size – caused numerous inflammatory cells to appear around the particle agglomerates and for macrophage-based phagocytosis to be induced. Long-term inflammatory reactions were stimulated by 0.5- and 3-μm Ti particles. As dissolution from particles was undetected *in vitro*, the main effects caused by Ti in rats appeared to be caused by the particles themselves rather than by ions. These results *in vivo* can be explained by assuming an increased release of superoxide, TNF-α and IL-1β, and subsequent cytotoxic stimulation in the soft tissue around the inserted Ti particles.

9.4.3
Comparison of Ti, Fe, and Ni Particles

In order to verify whether the cytotoxicity of fine particles originated from dissolved ions or from the particles *per se*, ICP elemental analyses were carried with HBSS containing Ti particles. Dissolution from Ti particles was below the limits of detection and negligible, which inferred that Ti was chemically stable and insoluble, whereas Fe was easily dissolved [23–26]. By contrast, Ni was seen to dis-

solve to some extent and hence to be highly toxic. Data acquired with regards to TNF-α release (see Fig. 9.7) indicated that Ti and Fe – both of which are biocompatible or are minimally cytotoxic when in macroscopic form (see Fig. 9.1) – demonstrated quantitatively similar size dependencies, despite Ti being insoluble and Fe soluble in HBSS. This lack of cytotoxicity by Ti and Fe, coupled with a lack of Ti dissolution, strongly suggested that any cytotoxicity related to the Ti and Fe particles was due to their physical size and not to the presence of dissolved ions. Ni showed a similar size-dependency, although the values of cell survival rate, superoxide anion and cytokine release were lowered. Significantly lower cell survival rates and higher LDH activities suggested that cell destruction occurred with a higher probability following exposure to Ni particles, and this might surpass the stimulatory effect of Ni and lower superoxide anion and IL-1β production. Previous results obtained with macroscopic Ni inserted into the soft tissue showed that necrosis and inflammation occurred which was dependent upon the distance from the Ni surface, though is also the function of concentration of dissolved Ni ions, as analyzed by XSAM [23–26]. The extreme toxicity of Ni was shown to originate from its dissolved ions.

9.4.4
The Effect of Micro-/Nanosizing on Biological Reactions

In general, the biocompatibility of a material depends on the chemical solubility of its ions, followed by its absorption into the cells and tissues. Corrosion resistance [27] is, therefore, a prerequisite for biomaterials, and this holds true for most materials of macroscopic size.

The effects of micro-/nanosizing are often explained in terms of their specific surface area, which increases in reciprocally proportional manner to particle size. The enhancement of chemical reactivity based on ionic dissolution can be more easily understood by this effect, an example of which is the accelerated toxicity of Ni (see Fig. 9.15), with tumor being generated after the long-term implantation of 0.5-μm particles, compared to necrosis in the short term. Other effects of changes in material properties when nanosizing include the increasing effect of the ratio of surface constituent atoms, and the quantum effect. All of these effects may be classified as the effects of the material itself.

The effects of micro/nanosizing also depend upon the size relationship between cells/tissues and particles. Physical particle size and shape effects occur non-specifically in many materials, and are unaffected by surface area effects. Such effects also seem to occur more easily in bioactive and bioinert materials, which are minimally influenced by chemical dissolution and show good biocompatibility on the macroscopic scale (as is the case for Ti and Fe; see Fig. 9.1). Thus, toxicity levels may be 10^3- to 10^4-fold lower than with endotoxins. Although this may not cause serious problems in the short term and in small quantities, it still causes inflammation *in vivo*, despite *in-vitro* toxicity being low. This situation would be serious when numbers of fine particles increase in quantity with time, and remain present over the long term; an example would be an artificial joint.

the lifetime of which is limited by the inflammation induced by abraded particles. A similar effect is seen with asbestos, where the long-term phagocytosis of acicular particles leads to chronic inflammation, together with superoxide production, defect formation in DNA, and carcinogenesis.

9.4.5 Terminology on "Nanotoxicology"

The term "Nanotoxicology" does not necessarily accurately reflect the effects caused by the particles described above. In biology, the size of the fundamental unit – the cell – is approximately 10 μm, and particle effects are pronounced in the range of 3 μm to 0.5 μm. However, particles < 50 nm in size may invade the body directly, via either the respiratory or digestive system, without stimulating the biophylactic system. Changes in function occurring over this size range are seen with hydroxyapatite, which is not only osteoconductive but also non-absorbable on a macroscopic scale, and is thus suited to biostructural implantation. Consequently, as apatite nanoparticles can form composites with collagen, apatite may function as a bone substitute, inducing absorption of the composite by osteoclasts and new bone formation by osteoblasts [28, 29]. Thus, particle effects on biological reactions may indeed be termed "micro/nanotoxicology".

Acknowledgments

These studies were conducted with financial support from Health and Labour Sciences Research Grants of the Research on Chemical Substance Assessment from the Ministry of Health, Labour and Welfare of Japan (H18-Chemistry-General-006).

References

1 H. Matsuno, A. Yokoyama, F. Watari, M. Uo, T. Kawasaki, *Biomaterials* **2001**, *22*, 1253–1262.
2 M. Uo, K. Asakura, A. Yokoyama, K. Tamura, Y. Totsuka, T. Akasaka, F. Watari, *Chem. Lett.* **2005**, *34*, 776–777.
3 Y. Tamura, A. Yokoyama, F. Watari, M. Uo, T. Kawasaki, *Mater. Trans.* **2002**, *43*, 3043–3051.
4 Y. Tamura, A. Yokoyama, F. Watari, T. Kawasaki, *Dent. Mater. J.* **2002**, *21*, 355–372.
5 F. Watari, A. Yokoyama, M. Omori, T. Hirai, H. Kondo, M. Uo, T. Kawasaki, *Composites Sci. Tech.* **2004**, *64*, 893–908.
6 K. Tamura, N. Takashi, R. Kumazawa, F. Watari, Y. Totsuka, *Mater. Trans.* **2002**, *43*, 3052–3057.
7 R. Kumazawa, F. Watari, N. Takashi, Y. Tanimura, M. Uo, Y. Totsuka, *Biomaterials* **2002**, *23*, 3757–3764.
8 K. Kiura, Y. Sato, M. Yasuda, B. Fugetsu, F. Watari, K. Tohji, K. Shibata, *J. Biomed. Nanotech.* **2005**, *1*, 359–364.
9 I.D. Rosca, F. Watari, M. Uo, T. Akasaka, *Carbon* **2005**, *43*, 3124–3131.

Handbook of Biomineralization. Edited by M. Epple and E. Bäuerlein
Copyright © 2007 WILEY-VCH Verlag GmbH & Co. KGaA, Weinheim
ISBN: 978-3-527-31806-3

10 M. Ushiro, K. Uno, T. Fujikawa, Y. Sato, K. Tohji, F. Watari, W.J. Chun, Y. Koike, K. Asakura, *Phys. Rev. B* **2006**, *73*, 144103/1–11.
11 K. Asakura, W.J. Chun, K. Tohji, Y. Sato, F. Watari, *Chem. Lett.* **2005**, *34*, 382–383.
12 B. Fugetsu, S. Satoh, T. Shiba, T. Mizutani, Y. Lin, N. Terui, Y. Nodasaka, K. Sasa, K. Shimizu, T. Akasaka, M. Shindoh, K. Shibata, A. Yokoyama, M. Mori, K. Tanaka, Y. Sato, K. Tohji, S. Tanaka, N. Nishi, F. Watari, *Environ. Sci. Technol.* **2004**, *38*, 6890–6896.
13 B. Fugetsu, S. Satoh, A. Iles, K. Tanaka, N. Nishi, F. Watari, *The Analyst (London)* **2004**, *129*, 565–566.
14 T. Akasaka, F. Watari, *Chem. Lett.* **2005**, *34*, 826–827.
15 T. Akasaka, F. Watari, Y. Sato, K. Tohji, *Mater. Sci. Eng. C* **2005**, *26*, 675–678.
16 N. Aoki, A. Yokoyama, Y. Nodasaka, T. Akasaka, M. Uo, Y. Sato, K. Tohji, F. Watari, *Chem. Lett.* **2006**, *35*, 508–509.
17 N. Aoki, A. Yokoyama, Y. Nodasaka, T. Akasaka, M. Uo, Y. Sato, K. Tohji, F. Watari, *J. Biomed. Nanotechnol.* **2005**, *1*, 402–405.
18 A. Yokoyama, Y. Sato, Y. Nodasaka, S. Yamamoto, T. Kawasaki, M. Shindoh, T. Kohgo, T. Akasaka, M. Uo, F. Watari, K. Tohji, *Nano Lett.* **2005**, *5*, 157–161.
19 Y. Sato, A. Yokoyama, K. Shibata, Y. Akimoto, S. Ogino, Y. Nodasaka, T. Kohgo, K. Tamura, T. Akasaka, M. Uo, K. Motomiya, B. Jeyadevan, M. Ishiguro, R. Hatakeyama, F. Watari, K. Tohj, *Mol. BioSystems* **2005**, *1*, 176–182.
20 Y. Sato, T. Shibata, H. Kataoka, S. Ogino, B. Fugetsu, A. Yokoyama, K. Tamura, T. Akasaka, M. Uo, K. Motomiya, B. Jeyadevan, R. Hatakeyama, F. Watari, K. Tohji, *Mol. BioSystems* **2005**, *1*, 142–145.
21 W. Wang, M. Omori, F. Watari, A. Yokoyama, *Dent. Mater. J.* **2005**, *24*, 478–486.
22 M. Uo, K. Tamura, Y. Sato, A. Yokoyama, F. Watari, Y. Totsuka, K. Tohji, *Small* **2005**, *1*, 816–819.
23 M. Uo, F. Watari, A. Yokoyama, H. Matsuno, T. Kawasaki, *Biomaterials* **2001**, *21*, 677–685.
24 M. Uo, F. Watari, A. Yokoyama, H. Matsuno, T. Kawasaki, *Biomaterials* **2001**, *22*, 1787–1794.
25 M. Uo, F. Watari, A. Yokoyama, H. Matsuno, T. Kawasaki, *Biomaterials* **1999**, *20*, 747–755.
26 M. Uo, K. Asakura, T. Kohgo, F. Watari, *Chem. Lett.* **2006**, *35*, 66–67.
27 F. Watari, *J. Electron Microsc.* **2005**, *54*, 299–308.
28 A. Yokoyama, M. Gelinsky, T. Kawasaki, T. Kohgo, U. Konig, W. Pompe, F. Watari, *J. Biomed. Mater. Res. B: Appl. Biomater.* **2005**, *75B*, 464–472.
29 S. Liao, W. Wang, M. Uo, S. Ohkawa, T. Akasaka, K. Tamura, F. Cui, F. Watari, *Biomaterials* **2005**, *26*, 7564–7571.